Analytical homogenization method for periodic composite materials

Ying Chen and Christopher A. Schuh*
Department of Materials Science and Engineering, Massachusetts Institute of Technology, 77 Massachusetts Avenue, Cambridge, Massachusetts 02139, USA

(Received 28 August 2008; revised manuscript received 23 January 2009; published 10 March 2009)

We present an easy-to-implement technique for determining the effective properties of composite materials with periodic microstructures, as well as the field distributions in them. Our method is based on the transformation tensor of Eshelby and the Fourier treatment of Nemat-Nasser *et al.* of this tensor, but relies on fewer limiting assumptions as compared to prior approaches in the literature. The final system of linear equations, with the unknowns being the Fourier coefficients for the potential, can be assembled easily without *a priori* knowledge of the concepts or techniques used in the derivation. The solutions to these equations are exact to a given order, and converge quickly for inclusion volume fractions up to 70%. The method is not only theoretically rigorous but also offers flexibilities for numerical evaluations.

DOI: 10.1103/PhysRevB.79.094104 PACS number(s): 72.80.Tm, 66.30.−h, 46.15.−x, 45.10.−b

I. INTRODUCTION

The effective properties of composite materials are determined by the statistical distribution of their constituent phase properties and the spatial distribution of the phases. Usually a volumetric average of individual phase properties represents the lowest-order approximation to the effective properties, while geometric factors provide second- and higher-order corrections.[1,2] The corrections are critical for essentially all nonparallel microstructures, but are unfortunately difficult to ascertain for complicated microstructural arrangements. Although substantial efforts have been made to solve for many mathematically analogous effective properties[3] such as electrical and thermal conductivity, dielectric constant, mass diffusivity, and magnetic permeability, understanding of geometric effects remains limited.

Among the simplest heterogeneous continuum microstructures are those with periodically distributed inclusions. Periodic composite materials can be completely specified by the phase distribution in one unit cell which is repeated periodically in space. Periodicity not only significantly simplifies the microstructure representation, but even permits analytical homogenization procedures. These procedures can be used to predict the effective properties of some real microstructures that can be approximated as periodic, e.g., the transverse sections of some fiber-reinforced composites. These analytical homogenization procedures can also be potentially useful for extrapolating the properties of nonperiodic composite materials of physically meaningful size. Assuming a periodic stacking of a representative volume element (RVE) might be a more accurate and efficient method than representing the composite with the RVE itself,[4] particularly when the convergence with respect to the RVE size is slow.

Existing methods (e.g., Refs. 5–16) for deriving the effective properties of periodic composite materials mostly rely on representations in the Fourier space. Using the Fourier expansion of the potential or field can automatically satisfy the continuity boundary conditions that are otherwise difficult to solve, and can also convert an integral equation into a system of linear equations for the unknown Fourier coefficients. For example, Helsing[8] expanded a displacement descriptor (force density) in a Fourier series and solved the resulting set of linear equations for the Fourier coefficients. Bergman and Dunn[5] and Cohen and Bergman[6] used the Fourier expansion for displacements, but they progressively tightened the upper and lower bounds instead of directly solving for the Fourier coefficients. Nemat-Nasser *et al.*[9,10] calculated the overall elastic properties of materials with periodically distributed inclusions or voids by expanding the Eshelby transformation strain tensor[17] in the Fourier series.

In solving for the elastic field of an inclusion embedded in an infinite matrix, Eshelby[17] introduced a transformation strain in the inclusion region so that, with the modified strain, the stress-strain relationships everywhere could be described by only the elastic constants of the matrix material. For periodic composite materials, Nemat-Nasser *et al.*[9,10] expressed the spatially varying transformation strain as well as other fields in the Fourier series and derived an integral equation from consistency and equilibrium requirements. The idea of Nemat-Nasser and co-workers is theoretically rigorous and conceptually straightforward. Consequently, the idea has been subsequently used for a variety of specific problems, such as the elastic properties of solids with periodically distributed cracks[18] and of periodic masonry structures,[19] elastic stiffness and the relaxation moduli of linear viscoelastic periodic composites,[20,21] the overall stress-strain relations of rate-dependent elastic-plastic periodic composites,[22] electrical conductivity,[23] thermal conductivity,[24] dielectric, elastic, and piezoelectric constants of periodic piezoelectric composites,[25] and the dielectric response of isotropic graded composites.[26]

However, the original derivations of the transformation field method[9,10] contain one considerably simplifying assumption, which has propagated through the line of works mentioned above (e.g., Refs. 9, 10, 18, 22, and 27). The simplification arises in deriving the relationship between the Fourier coefficients for the transformation strain and those for the true deformation field. The equilibrium condition has not been interpreted strictly [Eq. (2.5) became Eq. (2.8) in Ref. 9]. Specifically, given an infinite summation that must be equal to zero, it was assumed that each individual term in the summation should be equal to zero. Consequently, the

two essential features, the infinite summation and the position dependence in particular, in the original equation have been discarded. Moreover, the series for the transformation and perturbation strain have different numbers of terms, with the former including (and the latter excluding) the constant term corresponding to the reciprocal vector (0, 0, 0). Due to these issues, the final solution obtained by individually setting each term equal to zero might not be the true general solution. Discarding the infinite summation could result in larger deviations from the true solution for more complicated problems such as piezoelectric composites which require simultaneous solution of two governing equations.

In addition to the above considerations, in the original work of Nemat-Nasser and co-workers,[9,10] several approximations to the spatial distribution of the transformation strain were proposed in order to solve the equations. The one used most frequently by later authors is the assumption of a constant or piecewise-constant transformation strain within the inclusions. This assumption neglects the interactions among inclusions, which are significant at moderate to high inclusion volume fractions and can make the transformation strain position dependent. Another solution method recommended was to additionally expand the transformation strain as a polynomial series and solve for the polynomial coefficients. This method is not theoretically efficient since it involves an additional power series besides the initial Fourier series. The "complete solution method," which does not rely on any assumption on the distribution of the transformation strain and is thus most accurate among all the solution methods proposed, has, however, seldom been used, probably because of the difficulty in assembling or solving the system of linear equations.

In this paper, we adopt prior ideas of expanding the imaginary transformation "strain" in the Fourier series and building the equations from consistency and equilibrium requirements, but we derive the equations in a different, rigorous way, without making any assumptions that oversimplify the solution or render it accurate only for special circumstances. We show that, with the equations built properly, we can implement the "complete solution method" easily and obtain the Fourier coefficients (and hence the effective properties) efficiently. The results are exact to a given order and close to convergence approximately at the tenth order, which is computationally achievable. The method is in theory applicable to any microgeometry in a cuboid unit cell, and applies most easily for a single centered inclusion contained in a cubic unit cell. We present numerical results for cubic arrays of spherical and cubic inclusions, and further compare with some data adapted from the literature.

II. FORMULATION

In this section, we derive the effective diffusivity of periodic composite materials using Eshelby's concept of the transformation field[17] and the Fourier series representation of the field.[9] For clarity, the equations presented in the following are written for composites with isotropic diffusion properties, i.e., the diffusivity tensor for each phase reduces to a scalar, but the same procedure should apply to anisotropic constituent properties as well. The unit cell is a rectangular prism with dimensions L_1, L_2, and L_3 along the Cartesian coordinate axes. The total volume of the unit cell, $V=L_1L_2L_3$, is partitioned into the matrix region V_M and the inclusion region V_I, with $V=V_M+V_I$. The phase boundaries are assumed to be perfectly bonded.

A. Perturbation and transformation fields in Fourier series

Consider an infinite isotropic material with diffusivity D_M placed in a concentration field $C^0(\vec{R})$ that induces a uniform concentration gradient $E^0=-\nabla C^0(\vec{R})$, with E^0 the diffusion driving force and $\vec{R}=(x_1,x_2,x_3)$ the position vector in three dimensions. Inserting a periodic distribution of isotropic inclusions with diffusivity D_I into the matrix changes the concentration field to $C(\vec{R})=C^0(\vec{R})+C^d(\vec{R})$ and the concentration gradient to $E(\vec{R})=E^0+E^d(\vec{R})$, where $C^d(\vec{R})$ and $E^d(\vec{R})$ are the perturbations due to the insertion of inclusions, and $E^d(\vec{R})=-\nabla C^d(\vec{R})$. Because the inclusion distribution is periodic, both $C^d(\vec{R})$ and $E^d(\vec{R})$ are periodic functions with periodicity L_α in the $\alpha(\alpha=1,2,3)$ direction. Therefore, the actual concentration field $C(\vec{R})$ can be split into a linear part $C^0(\vec{R})$ and a periodic part $C^d(\vec{R})$, and accordingly, the concentration gradient $E(\vec{R})$ comprises a constant vector $E^0=(E_1^0,E_2^0,E_3^0)$ and a periodic vector $E^d(\vec{R})=[E_1^d(\vec{R}),E_2^d(\vec{R}),E_3^d(\vec{R})]$. Since the periodicity of $C^d(\vec{R})$ guarantees the periodicity of $E^d(\vec{R})$ while the converse is not necessarily true [e.g., a constant $E^d(\vec{R})$ would indicate a linear, instead of periodic, $C^d(\vec{R})$], we first write $C^d(\vec{R})$ as a Fourier series,

$$C^d(\vec{R})=\sum_{\xi}\hat{C}^d(\xi)e^{i\xi\cdot\vec{R}}, \tag{1}$$

where the reciprocal vector $\xi=(\xi_1,\xi_2,\xi_3)=(2\pi n_1/L_1,2\pi n_2/L_2,2\pi n_3/L_3)$ with n_1, n_2, $n_3=0,\pm1,\pm2,\ldots$. Then the perturbation in the gradient in the α direction, $E_\alpha^d(\vec{R})$, is proportional to the partial derivative of Eq. (1) with respect to x_α, the α_{th} component of $\vec{R}$,

$$E_\alpha^d(\vec{R})=-i\sum_{\xi}{}'\xi_\alpha\hat{C}^d(\xi)e^{i\xi\cdot\vec{R}}, \tag{2}$$

where the prime on the summation symbol Σ'_ξ denotes a summation excluding $\xi=(0,0,0)$, because the term $\hat{C}^d(\xi=(0,0,0))$ in Eq. (1) does not contribute to the differentiation with respect to position.

The diffusional flux in the composite in the α direction, $J_\alpha(\vec{R})$, is

$$J_\alpha(\vec{R})=\begin{cases}D_M[E_\alpha^0+E_\alpha^d(\vec{R})] & \text{in } V_M\\ D_I[E_\alpha^0+E_\alpha^d(\vec{R})] & \text{in } V_I.\end{cases} \tag{3}$$

Now, introduce a transformation gradient $E^*(\vec{R})$ so that with the modified concentration gradient $E^0+E^d(\vec{R})-E^*(\vec{R})$, the whole composite can be described with the diffusivity of the matrix material, D_M, everywhere,

$$J_\alpha(\vec{R}) = D_M[E^0_\alpha + E^d_\alpha(\vec{R}) - E^*_\alpha(\vec{R})]. \quad (4)$$

The equivalence between Eqs. (3) and (4) defines the transformation gradient $E^*(\vec{R})$ as

$$E^*_\alpha(\vec{R}) = \begin{cases} 0 & \text{in } V_M \\ (1 - D_I/D_M)[E^0_\alpha + E^d_\alpha(\vec{R})] & \text{in } V_I. \end{cases} \quad (5)$$

Because of the geometric periodicity, $E^*(\vec{R})$ is also periodic and can be written as a Fourier series as well,

$$E^*_\alpha(\vec{R}) = \sum_\xi \hat{E}^*_\alpha(\xi) e^{i\vec{\xi}\cdot\vec{R}} \quad (6)$$

with each Fourier coefficient being

$$\hat{E}^*_\alpha(\xi) = \frac{1}{V}\int_V E^*_\alpha(\vec{R}) e^{-i\vec{\xi}\cdot\vec{R}} d\vec{R} = \frac{1}{V}\int_{V_I} E^*_\alpha(\vec{R}) e^{-i\vec{\xi}\cdot\vec{R}} d\vec{R}, \quad (7)$$

where $d\vec{R}$ denotes $dx_1 dx_2 dx_3$. The second equality in Eq. (7) results from the fact that $E^*(\vec{R})$ is always zero for any $\vec{R}$ in V_M according to Eq. (5).

Because the normal component of the diffusional flux J has to be continuous across phase boundaries, $E^d(\vec{R})$ in Eqs. (3)–(5) may be discontinuous in certain direction(s). The transformation gradient $E^*(\vec{R})$ in Eq. (5) is also not necessarily continuous. The Fourier series for $E^d(\vec{R})$ in Eq. (2) and that for $E^*(\vec{R})$ in Eq. (6) thus represent discontinuous functions, and require many high-order terms in order to capture the discontinuities. However, as will be shown in the following subsections, our derivation for the effective diffusivity is based on the integration of the fields rather than the specific field distributions, and as such may actually converge faster than the spatial distribution of the fields themselves. The above definitions of $E^d(\vec{R})$ and $E^*(\vec{R})$ are analogous to the perturbation strain and transformation strain defined in the work of Nemat-Nasser *et al.*[9] In the following, we introduce a more rigorous method to solve for the Fourier coefficients for the above two series.

B. Solution technique

Replacing $E^d_\alpha(\vec{R})$ in Eq. (5) with the Fourier series in Eq. (2), we have

$$E^*_\alpha(\vec{R}) = (1 - D_I/D_M)\left[E^0_\alpha - i\sum_{\xi'}{}' \xi'_\alpha \hat{C}^d(\xi') e^{i\vec{\xi}'\cdot\vec{R}}\right] \quad \text{in } V_I. \quad (8)$$

Here the original symbol ξ in Eq. (2) is changed to ξ', which is the same reciprocal vector as ξ. $\xi' = (\xi'_1, \xi'_2, \xi'_3) = (2\pi n'_1/L_1, 2\pi n'_2/L_2, 2\pi n'_3/L_3)$ with n'_1, n'_2, $n'_3 = 0, \pm 1, \pm 2\ldots$. Multiplying both sides of Eq. (8) by $e^{-i\vec{\xi}\cdot\vec{R}}$ and integrating $\vec{R}$ over V_I, we have

$$\int_{V_I} E^*_\alpha(\vec{R}) e^{-i\vec{\xi}\cdot\vec{R}} d\vec{R} = (1 - D_I/D_M)\left[E^0_\alpha \int_{V_I} e^{-i\vec{\xi}\cdot\vec{R}} d\vec{R} - i\sum_{\xi'}{}' \xi'_\alpha \hat{C}^d(\xi') \int_{V_I} e^{-i(\vec{\xi}-\vec{\xi}')\cdot\vec{R}} d\vec{R}\right]. \quad (9)$$

The left side of Eq. (9) is equal to $V\hat{E}^*_\alpha(\xi)$ according to Eq. (7). As a result,

$$\hat{E}^*_\alpha(\xi) = f_I(1 - D_I/D_M)\left[E^0_\alpha g_{V_I}(\xi) - i\sum_{\xi'}{}' \xi'_\alpha g_{V_I}(\xi - \xi')\hat{C}^d(\xi')\right], \quad (10)$$

where $f_I = V_I/V$ is the inclusion volume fraction, and the geometric factor $g_{V_I}(\xi)$ is

$$g_{V_I}(\xi) = \frac{1}{V_I}\int_{V_I} e^{-i\vec{\xi}\cdot\vec{R}} d\vec{R}. \quad (11)$$

Equation (10) provides the connection between the Fourier coefficients for the transformation gradient, $\hat{E}^*_\alpha$, and the Fourier coefficients for the perturbation concentration field, $\hat{C}^d$. Here, in our method, each $\hat{E}^*_\alpha(\xi)$ value is an infinite summation over terms containing $\hat{C}^d(\xi')$, in contrast to the treatments used in prior works (e.g., Ref. 9) which would suggest, incorrectly, that each $\hat{E}^*_\alpha(\xi)$ can be fully determined by the corresponding $\hat{C}^d(\xi)$ with the same reciprocal vector ξ.

The steady-state condition requires that $\nabla \cdot J(\vec{R}) = 0$. Using the expression for $J(\vec{R})$ in Eq. (4), we obtain

$$\nabla \cdot [E^d(\vec{R}) - E^*(\vec{R})] = 0. \quad (12)$$

We substitute $E^d_\alpha(\vec{R})$ and $E^*_\alpha(\vec{R})$ in Eq. (12) with the series expression in Eqs. (2) and (6), respectively,

$$\sum_\xi{}' [(\xi \cdot \xi) i\hat{C}^d(\xi) + \xi \cdot \hat{E}^*(\xi)] e^{i\vec{\xi}\cdot\vec{R}} = 0, \quad (13)$$

where $\hat{E}^*(\xi) = [\hat{E}^*_1(\xi), \hat{E}^*_2(\xi), \hat{E}^*_3(\xi)]$. We multiply both sides of Eq. (13) by $e^{-i\vec{\eta}\cdot\vec{R}}$ and integrate $\vec{R}$ over an arbitrary volume Ω,

$$\sum_\xi{}' [(\xi \cdot \xi) i\hat{C}^d(\xi) + \xi \cdot \hat{E}^*(\xi)] g_\Omega(\eta - \xi) = 0, \quad (14)$$

where the geometric integration function g has already been defined in Eq. (11). This procedure introduces into the equation a virtual vector $\eta = (2\pi m_1/L_1, 2\pi m_2/L_2, 2\pi m_3/L_3)$, where m_1, m_2, and m_3 can be any integer, and a virtual integration volume Ω. As Eq. (13) holds for any $\vec{R}$ in the unit cell, the integration can be carried out over any finite volume Ω inside the unit cell in order to convert Eq. (13) to the position-independent Eq. (14). Ω is not restricted to be the inclusion volume V_I or unit-cell volume V, and this flexibility ensures the equivalence between Eq. (13) and Eq. (14). We however avoid assigning Ω as the unit-cell volume V because the integration of $e^{i(\eta-\xi)\cdot\vec{R}}$ over V is zero for any ξ

$\neq \eta$. Instead, we choose Ω in the range $V_I \leq \Omega < V$.

Replacing components of $\hat{E}^*(\xi)$ in Eq. (14) with Eq. (10) results in a linear equation whose only unknowns are the $\hat{C}^d(\xi)$ values, the Fourier coefficients for the perturbation concentration field $C^d(\vec{R})$ in Eq. (1).

$$\sum_{\xi}{}' \left[\frac{(\xi \cdot \xi)\hat{C}^d(\xi)}{f_I(1-D_I/D_M)} - \sum_{\xi'}{}' (\xi \cdot \xi') g_{V_I}(\xi - \xi') \hat{C}^d(\xi') \right] g_\Omega(\eta - \xi)$$
$$= i \sum_{\xi}{}' (\xi \cdot E^0) g_{V_I}(\xi) g_\Omega(\eta - \xi). \quad (15)$$

In the second term on the left side of Eq. (15), we first exchange the symbols ξ and ξ' and then exchange the sequence of summation to make the outer summation the one over ξ.

$$\sum_{\xi}{}' \sum_{\xi'}{}' (\xi \cdot \xi') g_{V_I}(\xi - \xi') \hat{C}^d(\xi') g_\Omega(\eta - \xi)$$
$$= \sum_{\xi'}{}' \sum_{\xi}{}' (\xi' \cdot \xi) g_{V_I}(\xi' - \xi) \hat{C}^d(\xi) g_\Omega(\eta - \xi')$$
$$= \sum_{\xi}{}' \left[\sum_{\xi'}{}' (\xi' \cdot \xi) g_{V_I}(\xi' - \xi) g_\Omega(\eta - \xi') \right] \hat{C}^d(\xi). \quad (16)$$

Then we group the two terms on the left side of Eq. (15) and obtain the final equation for the unknowns $\hat{C}^d(\xi)$,

$$\sum_{\xi}{}' \left[\frac{(\xi \cdot \xi) g_\Omega(\eta - \xi)}{f_I(1-D_I/D_M)} - \sum_{\xi'}{}' (\xi' \cdot \xi) g_{V_I}(\xi' - \xi) g_\Omega(\eta - \xi') \right] \hat{C}^d(\xi)$$
$$= i \sum_{\xi}{}' (\xi \cdot E^0) g_{V_I}(\xi) g_\Omega(\eta - \xi), \quad (17)$$

where $\xi = (2\pi n_1/L_1, 2\pi n_2/L_2, 2\pi n_3/L_3)$, $\xi' = (2\pi n_1'/L_1, 2\pi n_2'/L_2, 2\pi n_3'/L_3)$; the summations in this expression run over all possible integer combinations for (n_1, n_2, n_3) and (n_1', n_2', n_3'), respectively, except (0,0,0). For certain phase geometries, Eq. (17) may be further reduced to a simpler analytical form. For example, the derivation for a cubic lattice of cubic inclusions is shown in the Appendix. Although a substantial reduction to the form of Eq. (A5) is possible, it is not certain at present whether further simplification is possible. Thus in the following, we solve for the unknowns numerically.

If the infinite series is truncated at the Nth order, n and n' can be any value among $0, \pm 1, \pm 2 \ldots \pm N$. As each n and n' can take $2N+1$ values, there are $(2N+1)^3 - 1$ ξ and ξ' vectors in the summations. Thus there are $(2N+1)^3 - 1$ unknown $\hat{C}^d(\xi)$ values in Eq. (17). Accordingly, we can choose $(2N+1)^3 - 1$ arbitrary η vectors to build a system of linear equations with a square coefficient matrix, as Eq. (17) leads to one equation for each independent η vector. The specific choices of the vector η and the integration volume Ω should not affect the solution, but their values affect the condition number of the coefficient matrix of the linear equations. (The condition number is the ratio between the maximal and minimal singular values of the coefficient matrix, and a lower number indicates a well-conditioned matrix and a reliable solution from matrix inversion.) As a result, we can obtain a well-conditioned coefficient matrix by choosing appropriate η and Ω at a specific inclusion volume fraction f_I and diffusivity contrast ratio D_I/D_M.

Our solution method presented above directly solves for the unknown Fourier coefficients from the governing equations without first approximating the fields to any simpler form, such as constant, piecewise constant, or polynomial position dependent, which have been widely used previously at the expense of accuracy or efficiency.[23] The method corresponds to the idea of the "complete solution method" proposed by Nemat-Nasser *et al.*,[9] but is, we believe, somewhat simpler and more transparent. We derived the correlation between the Fourier coefficients for the transformation field and those for the perturbation field, as presented in Eq. (10), from the definition of the transformation field in Eq. (5), which naturally connects the transformation field to the perturbation field. Then we constructed the governing equation from the equilibrium or steady-state condition. The series of works that followed the method of Nemat-Nasser and coworkers (e.g., Refs. 9, 10, 18–23, and 25–27) have worked in the opposite way, i.e., deriving the relationship from the equilibrium condition and constructing the governing equation from the definition of transformation field, and used the simplifications elaborated in Sec. I. Furthermore, we have introduced a parameter—the integration volume Ω—when we converted a position-dependent equation, Eq. (13), into a position-independent one, Eq. (14). In addition to contributing to theoretical thoroughness, Ω is also practically useful as it can be varied to optimize the conditioning of the coefficient matrix of the final linear equations; we will return to this issue later when we consider some example problems.

C. Effective diffusivity

The effective diffusivity of the composite, D_{eff}, is defined as

$$D_{\text{eff}} = \frac{\langle J_\alpha(\vec{R}) \rangle_V}{\langle E_\alpha^0 + E_\alpha^d(\vec{R}) \rangle_V}, \quad (18)$$

where $\langle\ \rangle_V$ denotes an average over the unit cell. Here α can be any direction in which the macroscopic applied concentration gradient $E_\alpha^0 \neq 0$. Introducing the expression for the flux $J(\vec{R})$ in Eq. (4) into Eq. (18),

$$D_{\text{eff}} = D_M \left(1 - \frac{\langle E_\alpha^*(\vec{R}) \rangle_V}{E_\alpha^0 + \langle E_\alpha^d(\vec{R}) \rangle_V} \right), \quad (19)$$

where

$$\langle E_\alpha^*(\vec{R}) \rangle_V = \frac{1}{V} \int_V E_\alpha^*(\vec{R}) d\vec{R}$$
$$= \hat{E}_\alpha^*[\xi = (0,0,0)]$$
$$= f_I(1 - D_I/D_M)$$

$$\times\left\{E^0_\alpha g_{V_I}[(0,0,0)] - i\sum_{\xi'}{}' \xi'_\alpha g_{V_I}(-\xi')\hat{C}^d(\xi')\right\}$$
$$= f_I(1 - D_I/D_M)\left[E^0_\alpha - i\sum_{\xi}{}' \xi_\alpha g_{V_I}(-\xi)\hat{C}^d(\xi)\right]. \quad (20)$$

In Eq. (20), the second equality is due to Eq. (7), the third is due to Eq. (10), and the fourth introduces a notation change from ξ' back to ξ in the second term. From Eq. (2), the volume average of $E^d_\alpha(\vec{R})$ vanishes because $\int_V e^{i\xi\cdot R}d\vec{R}=0$ for any $\xi\neq(0,0,0)$,

$$\langle E^d_\alpha(\vec{R})\rangle_V = \frac{1}{V}\int_V E^d_\alpha(\vec{R})d\vec{R} = -\frac{1}{V}i\sum_{\xi}{}' \xi_\alpha \hat{C}^d(\xi)\left(\int_V e^{i\xi\cdot\vec{R}}d\vec{R}\right)$$
$$= 0. \quad (21)$$

Introducing Eqs. (20) and (21) back into Eq. (19), we obtain an explicit expression for the effective diffusivity,

$$D_{\text{eff}} = (1-f_I)D_M + f_I D_I + \frac{f_I(D_M - D_I)}{E^0_\alpha} i\sum_{\xi}{}' \xi_\alpha g_{V_I}(-\xi)\hat{C}^d(\xi), \quad (22)$$

where the $\hat{C}^d(\xi)$ values are the solutions of the governing equation Eq. (17). In Eq. (22), the effective diffusivity consists of two parts, the first being a volumetric average of the matrix and inclusion diffusivities and the second being a series summation. The series summation results from the periodicity of the inclusion distribution, and depends on the inclusion geometry via the integration function g and the g-dependent $\hat{C}^d(\xi)$ values. Although Eq. (22) is derived using the transformation gradient $E^*_\alpha(\vec{R})$ which is specific to the present study, it is analogous to expressions for other effective transport properties in the literature, e.g., Refs. 5 and 28, because of the similar definitions of effective transport properties.

III. EXAMPLES AND DISCUSSION

In this section, we shall discuss the computational aspects of our method and examine the convergence of the effective diffusivity with respect to the truncation order N, the highest order in the Fourier series included in the calculation. We will also compare our results with the predictions from some other theories. We specifically evaluate the effective diffusivities of composite materials containing a cubic array of either cubic or spherical inclusions. In these cases the unit cell for the periodic composite is cubic so that $L_1=L_2=L_3=L$ in all previous equations in Sec. II.

A. Computation

The geometric factor g defined in Eq. (11) for a centered cuboid inclusion of volume V_I is

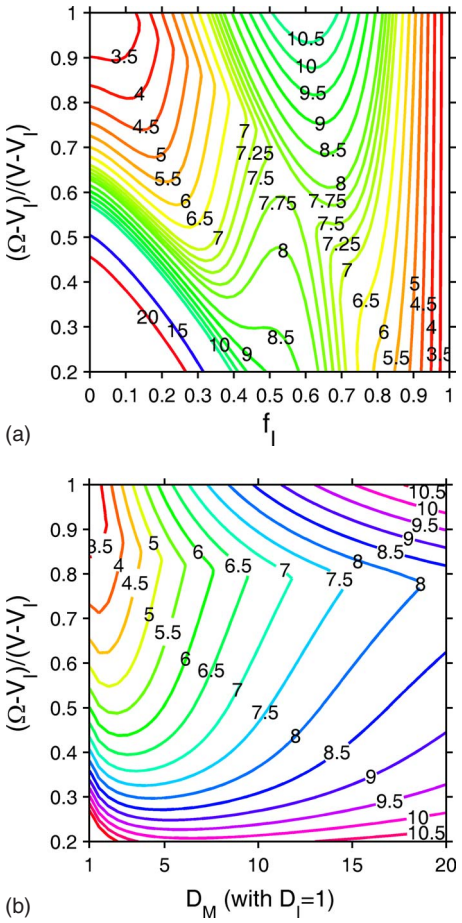

FIG. 1. (Color online) (a) Contour plot of the condition number of the coefficient matrix of Eq. (17) as a function of inclusion volume fraction f_I and normalized omega $(\Omega-V_I)/(V-V_I)$ when $D_M=10$ and $D_I=1$. (b) Contour plot of the condition number as a function of diffusivity contrast and normalized omega at $f_I=0.4$. Both figures are obtained from the lowest-order ($N=1$) calculations for a cubic array of cubic inclusions only to show the heterogeneity in the condition number due to the variations in Ω.

$$g_{V_I}(\xi) = \frac{1}{V_I}\int_{V_I} e^{-i\xi\cdot\vec{R}}d\vec{R} = \prod_{\alpha=1}^{3}\left(\frac{1}{L_{I\alpha}}\int_{-L_{I\alpha}/2}^{L_{I\alpha}/2} e^{-i\xi_\alpha x_\alpha}dx_\alpha\right), \quad (23)$$

where $L_{I\alpha}$ is the size of the inclusion in the α direction. Each multiplying term in Eq. (23) is

$$Y(\xi_\alpha) = \frac{1}{L_{I\alpha}}\int_{-L_{I\alpha}/2}^{L_{I\alpha}/2} e^{-i\xi_\alpha x_\alpha}dx_\alpha$$
$$= \begin{cases} 1 & \text{if } \xi_\alpha = 0 \\ \dfrac{2}{L_{I\alpha}\xi_\alpha}\sin\left(\dfrac{L_{I\alpha}\xi_\alpha}{2}\right) & \text{if } \xi_\alpha \neq 0. \end{cases} \quad (24)$$

For cubic inclusions, $L_{I1}=L_{I2}=L_{I3}=L_I$ in Eqs. (23) and (24).

The geometric factor g for a spherical inclusion with radius $r(4\pi r^3/3=V_I)$ is[9,28]

TABLE I. The effective diffusivities of composites containing a cubic array of cubic inclusions at various volume fractions f_I for different orders N. D_M and D_I are respectively diffusivities for the matrix and inclusion material.

N	f_I=0.1	0.2	0.3	0.4	0.5	0.6	0.7	0.8	0.9
				D_M=1, D_I=10 (D_I/D_M=10)					
0	1.9000	2.8000	3.7000	4.6000	5.5000	6.4000	7.3000	8.2000	9.1000
1	1.4207	2.0441	2.8971	3.9073	4.9851	6.0657	7.1151	8.1207	9.0811
2	1.3764	1.7491	2.2944	3.1424	4.2925	5.5904	6.8617	8.0209	9.0597
3	1.3412	1.7346	2.1458	2.7180	3.6620	5.0223	6.5333	7.8971	9.0357
4	1.3284	1.6932	2.1362	2.6134	3.3034	4.4933	6.1439	7.7460	9.0087
5	1.3162	1.6675	2.0961	2.6050	3.1826	4.1243	5.7352	7.5665	8.9785
6	1.3109	1.6621	2.0555	2.5772	3.1654	3.9342	5.3652	7.3606	8.9448
7	1.3043	1.6446	2.0495	2.5267	3.1568	3.8665	5.0798	7.1348	8.9071
8	1.3017	1.6407	2.0390	2.5000	3.1234	3.8536	4.8932	6.9006	8.8652
9	1.2973	1.6340	2.0210	2.4964	3.0756	3.8496	4.7904	6.6724	8.8189
10	1.2959	1.6275	2.0164	2.4877	3.0442	3.8318	4.7495	6.4647	8.7680
11	1.2928	1.6258	2.0124	2.4689	3.0358	3.7959	4.7331	6.2888	8.7124
12	1.2920	1.6201	2.0025	2.4577	3.0336	3.7539	4.7308	6.1500	8.6522
13	1.2896	1.6187	1.9989	2.4559	3.0237	3.7226	4.7266	6.0482	8.5875
				D_M=10, D_I=1 (D_I/D_M=0.1)					
0	9.1000	8.2000	7.3000	6.4000	5.5000	4.6000	3.7000	2.8000	1.9000
1	8.8720	7.7337	6.7117	5.7903	4.9397	4.1343	3.3554	2.5887	1.8183
2	8.8117	7.7126	6.6618	5.6743	4.7775	3.9637	3.2077	2.4844	1.7695
3	8.7940	7.6390	6.6114	5.6602	4.7535	3.9107	3.1431	2.4293	1.7387
4	8.7641	7.6298	6.5720	5.6212	4.7421	3.9005	3.1154	2.3975	1.7178
5	8.7593	7.6047	6.5657	5.5966	4.7184	3.8955	3.1062	2.3787	1.7030
6	8.7465	7.5980	6.5488	5.5918	4.6998	3.8841	3.1040	2.3679	1.6921
7	8.7425	7.5880	6.5383	5.5837	4.6931	3.8711	3.1016	2.3623	1.6839
8	8.7369	7.5815	6.5354	5.5725	4.6909	3.8617	3.0968	2.3599	1.6775
9	8.7331	7.5778	6.5273	5.5677	4.6856	3.8575	3.0906	2.3590	1.6726
10	8.7307	7.5719	6.5229	5.5660	4.6787	3.8562	3.0846	2.3585	1.6688
11	8.7273	7.5705	6.5211	5.5611	4.6744	3.8547	3.0801	2.3577	1.6659
12	8.7262	7.5662	6.5164	5.5566	4.6731	3.8516	3.0774	2.3561	1.6637
13	8.7234	7.5648	6.5141	5.5553	4.6718	3.8478	3.0762	2.3541	1.6620

$$g_{V_I}(\xi) = \frac{1}{V_I}\int_{V_I} e^{-i\xi\cdot\vec{R}} d\vec{R} = \begin{cases} 1 & \text{if } \xi = (0,0,0) \\ \dfrac{3}{(|\xi|r)^3}[\sin(|\xi|r) - |\xi|r\cos(|\xi|r)] & \text{if } \xi \neq (0,0,0). \end{cases} \tag{25}$$

The maximum radius of a sphere in the cubic unit cell is $r_{\max}=L/2$ so the maximum possible volume fraction of spherical inclusions in this case is $f_{I\max}=4\pi r_{\max}^3/(3L^3)=\pi/6\approx 0.5236$. Our method should work for overlapping spheres as well, except that the integration function g_{V_I} in Eqs. (17) and (22) can no longer be calculated from Eq. (25) and needs to be specifically evaluated.

For convenience, we confine η in Eq. (17) to be in the same range as ξ and ξ', i.e., $\eta = (2\pi m_1/L_1, 2\pi m_2/L_2, 2\pi m_3/L_3)$, where m_1, m_2, and $m_3=0$, ± 1, $\pm 2 \ldots \pm N$. Both the shape and the volume of Ω can be varied to simplify the integration or improve the conditioning of the coefficient matrix, although in principle, any choice of Ω should yield the same result. For example, for both cubic and spherical inclusions, using cubic and spherical shapes for Ω yields the same value of effective diffusivity. The final results we present in the following are calculated from cubic Ω for both cubic and spherical inclusions, thus the integration over Ω can be calculated from Eqs. (23) and (24) with V_I replaced by Ω.

The effect of the volume Ω is illustrated in Fig. 1 where we varied Ω between V_I and V for cubic inclusions and calculated the condition number of the coefficient matrix at different inclusion volume fractions f_I and diffusivity contrasts D_I/D_M. The vertical axis is normalized so that a value of 0 indicates integration over inclusion volume V_I while a value of 1 means integration over the unit-cell volume V. Both

TABLE II. The effective diffusivity for a cubic array of spherical inclusions at various volume fractions f_I for different orders N. D_M and D_I are, respectively, diffusivities for the matrix and inclusion material.

N	f_I=0.1	0.2	0.3	0.4	0.5
			D_M=1, D_I=10 (D_I/D_M=10)		
0	1.9000	2.8000	3.7000	4.6000	5.5000
1	1.3999	1.9941	2.7765	3.6742	4.6239
2	1.3354	1.7252	2.3618	3.2636	4.2820
3	1.3128	1.6594	2.1592	3.0046	4.0707
4	1.2935	1.6363	2.0684	2.8329	3.9306
5	1.2859	1.6170	2.0287	2.7146	3.8288
6	1.2785	1.6009	2.0086	2.6325	3.7510
7	1.2738	1.5911	1.9944	2.5765	3.6888
8	1.2703	1.5848	1.9818	2.5390	3.6379
9	1.2671	1.5790	1.9705	2.5140	3.5954
10	1.2651	1.5738	1.9610	2.4969	3.5590
11	1.2630	1.5701	1.9538	2.4847	3.5276
12	1.2615	1.5673	1.9486	2.4755	3.5002
13	1.2601	1.5645	1.9444	2.4680	3.4759
			D_M=10, D_I=1 (D_I/D_M=0.1)		
0	9.1000	8.2000	7.3000	6.4000	5.5000
1	8.8587	7.7018	6.6452	5.6527	4.6746
2	8.7953	7.6725	6.6091	5.6010	4.6022
3	8.7878	7.6556	6.5957	5.5834	4.5835
4	8.7818	7.6484	6.5880	5.5744	4.5745
5	8.7787	7.6447	6.5829	5.5691	4.5683
6	8.7768	7.6419	6.5795	5.5656	4.5639
7	8.7752	7.6398	6.5772	5.5630	4.5609
8	8.7743	7.6384	6.5755	5.5610	4.5585
9	8.7733	7.6373	6.5742	5.5594	4.5566
10	8.7728	7.6363	6.5730	5.5581	4.5551
11	8.7722	7.6355	6.5721	5.5570	4.5538
12	8.7718	7.6349	6.5713	5.5561	4.5527
13	8.7714	7.6344	6.5708	5.5554	4.5518

Figs. 1(a) and 1(b) are obtained from the lowest-order (N=1) calculations merely to show the heterogeneity in the condition number due to the variation in Ω. For all these different Ω values, we obtained the same effective diffusivity; this is the expected behavior of a correct solution. However, in other situations where the coefficient matrix is too ill conditioned to solve easily, the flexibility of choosing shapes and volumes for Ω might be useful for obtaining more reliable solutions.

The coefficient matrix in the governing equation Eq. (17) is a full matrix, but its requirements for computer memory and CPU time can be reduced either by attempting to further simplify Eq. (17) analytically, as demonstrated in the Appendix, or by making use of matrix operations and symmetries. As we show in Tables I and II, and will discuss at more length later, a truncation order N=10 produces reasonable results for most of our examples. At this order, even if all symmetries are ignored, the calculation would take only ~1 GB of memory and ~20 h using a personal computer if the coefficient matrix of the governing equations is assembled using row vectors instead of element by element, and would take ~2 GB of memory and ~8–10 h if column vectors are used instead [although Eq. (17) is presented on a row basis]. A quad-core computer would further reduce the computing time to ~2 h for this scenario and to only a few minutes if all calculations are based on matrix operations. The computational expense could be further reduced if symmetries are taken into account. We thus find that the computing cost is acceptable considering the accuracy and simplicity of the method.

B. Convergence

Table I presents the effective diffusivities calculated at an increasing truncation order N for composites containing a cubic array of cubic inclusions at various inclusion volume fractions f_I. For both diffusivity contrast ratios, D_I/D_M=10 and 0.1, the effective diffusivities calculated always decrease monotonically with increasing order N. This is because, as shown both in Eq. (22) and in the table, the zeroth-order solution is simply the linear average of phase diffusivities, $D_{\text{eff}}=(1-f_I)D_M+f_I D_I$, which is an upper bound. As we add more high-order terms, more interaction effects are progressively taken into account. The resulting diffusivities converge quite quickly as we increase the truncation order N for volume fractions $f_I<0.7$ when D_I/D_M=10 and for all fractions when D_I/D_M=0.1. When $D_I>D_M$, the interactions among inclusions become stronger at higher volume fractions, making it more difficult to achieve convergence; more high-order terms are needed in order to capture these strong interactions. On the other hand, the range of $f_I<0.7$ should cover inclusion volume fractions of most periodic composites, as an exceptionally high length ratio of L_I/L=0.9 only results in f_I=0.729.

The effective diffusivities for a cubic array of spherical inclusions are listed in Table II. The trends of convergence discussed above for cubic inclusions are also generally true here, except that the transition to a "high" volume fraction occurs much sooner for spheres than for cubic inclusions because the maximum volume fraction of nonoverlapping spheres is only about 0.52.

The data in Tables I and II for cubic and spherical inclusions, respectively, are also plotted in Fig. 2. Here it is easier to compare the convergence trends for the two inclusion geometries (data for cubic inclusions are plotted as squares while those for spherical inclusions are plotted as circles) and for different diffusivity ratios (D_I/D_M=10 in filled symbols on the left and D_I/D_M=0.1 in open symbols on the right). When D_I/D_M=10, D_{eff} for composites with spherical inclusions is lower than that for composites with cubic inclusions at f_I=0.1, 0.2, and 0.3, but becomes higher when f_I=0.4 and 0.5. This might be because at the same volume fraction, the minimum distance between spherical inclusions is much smaller than that between cubic inclusions. Since the diffusivity of the segregated inclusions is higher, the effec-

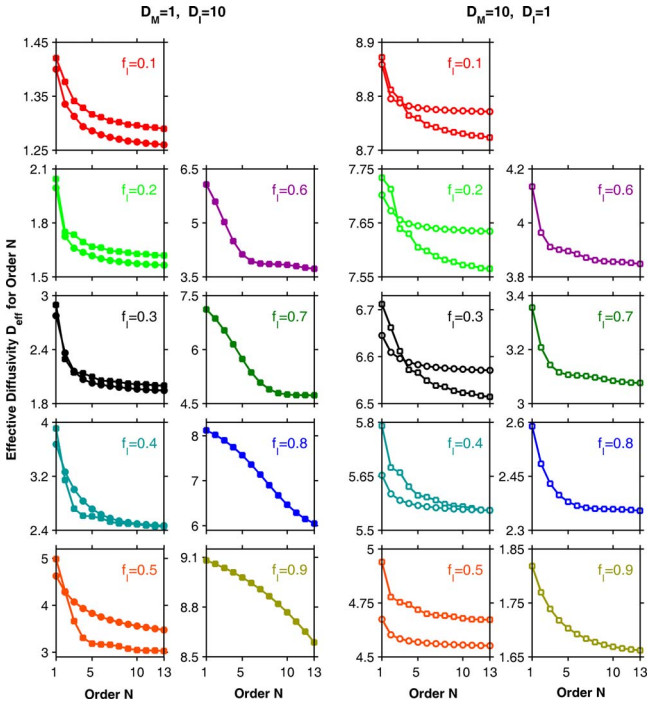

FIG. 2. (Color online) Convergence of the calculated effective diffusivity D_{eff} with respect to the truncation order N at various inclusion volume fractions f_I=0.1–0.9. The squares (■ and □) denote data for cubic inclusions while the circles (● and ○) are the data points for spherical inclusions. The filled symbols (■ and ●) are for the case of D_M=1 and D_I=10, and the open symbols (□ and ○) are for the case of D_M=10 and D_I=1.

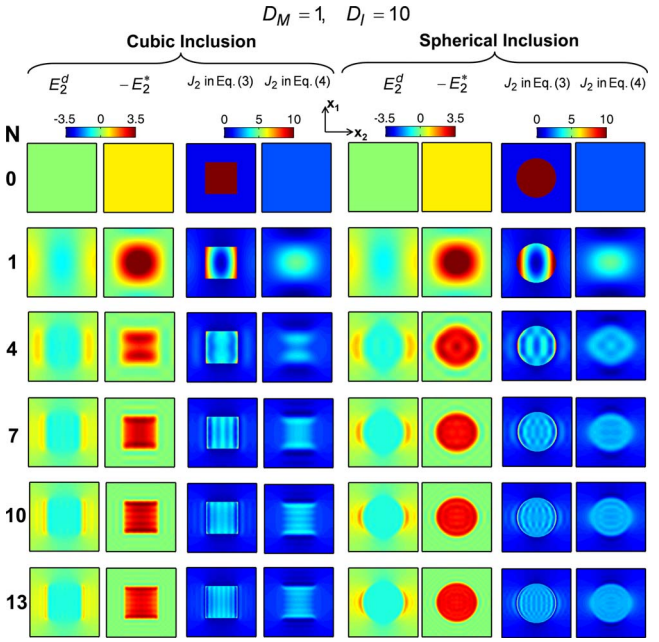

FIG. 3. (Color online) The distribution of perturbation field $E_2^d(\vec{R})$ defined in Eq. (2), transformation field $E_2^*(\vec{R})$ defined in Eq. (6), diffusional flux $J_2(\vec{R})$ in Eq. (3), and $J_2(\vec{R})$ in Eq. (4) under a unit applied diffusion driving force in the x_2 direction $[E^0=(0,1,0)]$ with increasing terminating order N of the Fourier series. Shown in the figure are the distribution of these fields on the symmetric plane $x_3=0$ $[\vec{R}=(x_1,x_2,0)]$ in the unit cell for cubic inclusion (left) and spherical inclusion (right) with matrix diffusivity D_M=1 and inclusion diffusivity D_I=10 at inclusion fraction f_I=0.1.

tive diffusivities of the composite material will be higher when the inclusions are closer to each other. This effect becomes evident at high volume fractions. It is the opposite case when D_I/D_M=0.1. Now the matrix phase becomes the main diffusion path and the narrow necks of the matrix material may limit the diffusional flow. Therefore D_{eff} for composites with spherical inclusions is higher than that for composites with cubic inclusions at f_I=0.1, 0.2, and 0.3, and then becomes lower when f_I=0.4 and 0.5.

The convergence with respect to the terminating order N of the partial sum of the Fourier series can be revealed by the spatial distributions of the solved fields as well. The distributions of the perturbation field $E_2^d(\vec{R})$ defined in Eq. (2), the transformation field $E_2^*(\vec{R})$ defined in Eq. (6), diffusional flux $J_2(\vec{R})$ defined in Eq. (3), and $J_2(\vec{R})$ defined in Eq. (4) are shown in Fig. 3 for the case of matrix diffusivity D_M=1 and inclusion diffusivity D_I=10 and in Fig. 4 for the opposite case, D_M=10 and D_I=1. In both Figs. 3 and 4, a unit diffusion driving force is applied in the x_2 direction $[E^0=(0,1,0)]$, and what are shown are the distributions of the fields on the symmetric plane $x_3=0$ $[\vec{R}=(x_1,x_2,0)]$ in the unit cell for cubic inclusion (left) and spherical inclusion (right) at inclusion fraction f_I=0.1. E^d reflects the perturbation in E^0 due to the insertion of a periodic distribution of inclusions. Its distribution pattern arises mainly because E^0 is in the x_2 direction, and it is almost zero in the matrix far from the inclusion. The distribution of E_2^* approaches the shape of the inclusion as N increases, and a convergence indicator is that E_2^* is only nonzero in the inclusion as suggested by Eq. (5). The increasing similarity between the distribution of J_2 in Eq. (3) and that of J_2 in Eq. (4) at high N indicates more convincingly the numerical results being close to convergence. As discussed at the end of Sec. II A, accurate representations of discontinuous functions by the Fourier series require a sufficient number of high-order terms. The resemblance between J_2 in Eq. (3) and J_2 in Eq. (4) at high N implies there are adequate terms in the partial sum of the Fourier series.

C. Comparison with other theories

In Table III, we compare the high-order numerical results in Tables I and II with predictions from some earlier models, including the Maxwell-Garnett (MG) formula, which coincides with the Hashin-Shtrikman (HS) bounds,[29] Rayleigh's method,[30] and McKenzie and McPhedran's model.[31,32] It is generally recognized that the MG formula, Rayleigh method, and McKenzie *et al.* model are of order 1, 2, and 4, respectively (the order here is different from the truncation order N used in our calculation).[31] The models of Rayleigh and McKenzie *et al.* are specifically derived for a cubic array of spheres.

When D_M=1 and D_I=10, our results are slightly above the predictions of the MG formula (or HS lower bound).

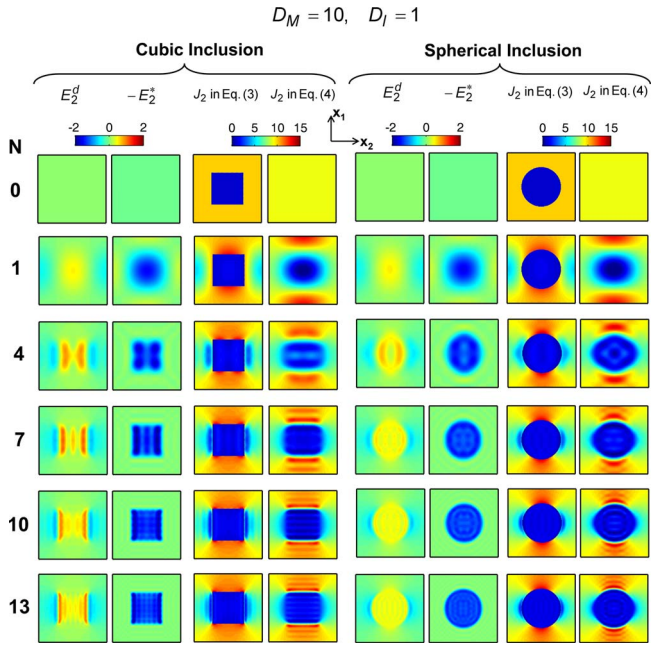

FIG. 4. (Color online) The distribution of perturbation field $E_2^d(\vec{R})$ defined in Eq. (2), transformation field $E_2^*(\vec{R})$ defined in Eq. (6), diffusional flux $J_2(\vec{R})$ defined in Eq. (3), and $J_2(\vec{R})$ defined in Eq. (4) under a unit applied diffusion driving force in the x_2 direction $[E^0=(0,1,0)]$ with increasing terminating order N of the Fourier series. Shown in the figure are the distribution of these fields on the symmetric plane $x_3=0$ $[\vec{R}=(x_1,x_2,x_3)]$ in the unit cell for cubic inclusion (left) and spherical inclusion (right) with matrix diffusivity $D_M=10$ and inclusion diffusivity $D_I=1$ at inclusion fraction $f_I=0.1$.

Both the matrix and the inclusion phases are isotropic and the diffusivity of the isolated inclusions is higher than the diffusivity of the surrounding matrix material so the microstructure is very close to the HS lower bound.[33] Comparing results from the method of Rayleigh, the model of McKenzie *et al.* and our results for spherical inclusions, it is seen that higher-order evaluations generally result in higher effective diffusivities. Although our results may vary a few thousandths considering the convergence trend shown in Tables I and II, the variation is marginal and this trend still holds. For the same type of composite microstructures, Gu *et al.*[23] also observed that predictions from homogenization approaches that include higher-order interactions are close to but somewhat above the lower bound for isotropic structures.

When $D_M=10$ and $D_I=1$, the results are very close to the HS upper bound because now the percolating matrix phase has a higher diffusivity. For cubic inclusions, our high-order results converge well to below the upper bound at volume fractions $f_I=0.1-0.7$, but seem to stay a little above the upper bound at $f_I=0.8$ and 0.9 even though convergence has almost been reached, as shown in Table I and Fig. 2. For spherical inclusions, although the results seem to have almost converged at all inclusion fractions (see Table II and Fig. 2), D_{eff} at $f_I=0.1$ and 0.2 remain slightly above the upper bound while D_{eff} at $f_I=0.3-0.5$ are below the upper bound.

IV. SUMMARY

In summary, we have proposed a technique for calculating the effective properties of composite materials with periodic microstructures and the field distributions in them. Numerical examples for a cubic array of cubic inclusions and spherical inclusions were presented and compared to the predictions from some existing homogenization theories. The method is rigorous, easy to use, and reasonably efficient. The solutions to the problem are exact to a given order and are converging. It is hoped that the present developments will encourage further numerical and analytical work on such microstructures, which have broad applicability across many of the physical sciences.

ACKNOWLEDGMENT

This work was supported by the U.S. National Science Foundation through Contract No. DMR-0346848.

APPENDIX: FURTHER ANALYTICAL SIMPLIFICATION OF THE GOVERNING EQUATION

As there is a high degree of element symmetry in Eq. (17), we can possibly further simplify the equation analytically. As an example, consider cubic inclusions. From the equations for the geometric integration $g_{V_I}(\xi_1,\xi_2,\xi_3)=\Pi_{\alpha=1}^3 Y(\xi_\alpha)$ in Eqs. (23) and (24), we can further obtain

$$\sum_{\xi'_\alpha} Y(\xi'_\alpha-\xi_\alpha)Y(\xi'_\alpha-\eta_\alpha)=\frac{L}{L_I}Y(\xi_\alpha-\eta_\alpha), \tag{A1}$$

$$\sum_{\xi'_\alpha} \xi'_\alpha Y(\xi'_\alpha-\xi_\alpha)Y(\xi'_\alpha-\eta_\alpha)=\frac{L}{L_I}\frac{\xi_\alpha+\eta_\alpha}{2}Y(\xi_\alpha-\eta_\alpha), \tag{A2}$$

if we retain all terms up to infinite order in the Fourier series. Equations (A1) and (A2) have been derived by making use of the Fourier expansions for the Bernoulli polynomials[34]

$$B_1(\theta)=\theta-\frac{1}{2}=-\frac{1}{\pi}\left[\sum_{n=1}^{\infty}\frac{\sin(2\pi n\theta)}{n}\right], \tag{A3}$$

$$B_2(\theta)=\theta^2-\theta+\frac{1}{6}=\frac{1}{\pi^2}\left[\sum_{n=1}^{\infty}\frac{\cos(2\pi n\theta)}{n^2}\right]. \tag{A4}$$

If we assume that the integration volume $\Omega=V_I$ and then introduce Eqs. (A1) and (A2) back into Eq. (17), we obtain

$$\sum_{\xi}{}' \left[\frac{D_I+D_M}{D_I-D_M}(\xi\cdot\xi)+(\xi\cdot\eta)\right]g_{V_I}(\xi-\eta)\hat{C}^d(\xi) = -i(\eta\cdot E^0)g_{V_I}(\eta). \tag{A5}$$

TABLE III. Comparison of our high-order results with predictions from other theories.

				Present Method	
f_I	First order (MG)	Second order (Rayleigh)	Fourth order (McKenzie and McPhedran[a])	Spherical inclusion	Cubic inclusion
			$D_M=1$, $D_I=10$ ($D_I/D_M=10$)		
0.1	1.2432	1.2433	1.2433	1.2601	1.2896
0.2	1.5294	1.5317	1.5317	1.5645	1.6187
0.3	1.8710	1.8870	1.8876	1.9444	1.9989
0.4	2.2857	2.3567	2.3631	2.4680	2.4559
0.5	2.8000	3.0532	3.1133	3.4759	3.0237
0.6	3.4545				3.7226
0.7	4.3158				4.7266
0.8	5.5000				6.0482↓
0.9	7.2308				8.5875↓
			$D_M=10$, $D_I=1$ ($D_I/D_M=0.1$)		
0.1	8.7671	8.7669	8.7669	8.7714	8.7234
0.2	7.6316	7.6280	7.6280	7.6344	7.5648
0.3	6.5823	6.5630	6.5632	6.5708	6.5141
0.4	5.6098	5.5468	5.5480	5.5554	5.5553
0.5	4.7059	4.5496	4.5519	4.5518	4.6718
0.6	3.8636				3.8478
0.7	3.0769				3.0762
0.8	2.3404				2.3541
0.9	1.6495				1.6620

[a]Reference 31.

*Corresponding author; schuh@mit.edu

[1] M. Sahimi, *Heterogeneous Materials 1: Linear Transport and Optical Properties* (Springer, New York, 2003).
[2] S. Torquato, *Random Heterogeneous Materials: Microstructure and Macroscopic Properties* (Springer, New York, 2002).
[3] G. K. Batchelor, Annu. Rev. Fluid Mech. **6**, 227 (1974).
[4] V. I. Kushch and I. Sevostlanov, Int. J. Solids Struct. **41**, 885 (2004).
[5] D. J. Bergman and K. J. Dunn, Phys. Rev. B **45**, 13262 (1992).
[6] I. Cohen and D. J. Bergman, J. Mech. Phys. Solids **51**, 1433 (2003).
[7] G. Bonnet, J. Mech. Phys. Solids **55**, 881 (2007).
[8] J. Helsing, J. Mech. Phys. Solids **43**, 815 (1995).
[9] S. Nemat-Nasser and M. Taya, Q. Appl. Math. **39**, 43 (1981).
[10] S. Nemat-Nasser, T. Iwakuma, and M. Hejazi, Mech. Mater. **1**, 239 (1982).
[11] P. Bisegna and R. Luciano, J. Mech. Phys. Solids **45**, 1329 (1997).
[12] J. C. Michel, H. Moulinec, and P. Suquet, Comput. Methods Appl. Mech. Eng. **172**, 109 (1999).
[13] V. I. Kushch, Proc. R. Soc. London, Ser. A **453**, 65 (1997).
[14] R. Tao, Z. Chen, and P. Sheng, Phys. Rev. B **41**, 2417 (1990).
[15] E. Pruchnicki, Int. J. Solids Struct. **35**, 1895 (1998).
[16] B. Yang, C. Zhang, Y. Zheng, T. Lu, X. Wu, W. Su, and S. Wu, Phys. Rev. B **58**, 14127 (1998).
[17] J. D. Eshelby, Proc. R. Soc. London, Ser. A **241**, 376 (1957).
[18] S. Nemat-Nasser, N. Yu, and M. Hori, Int. J. Solids Struct. **30**, 2071 (1993).
[19] G. Wang, S. Li, H.-N. Nguyen, and N. Sitar, J. Mater. Civ. Eng. **19**, 269 (2007).
[20] R. Luciano and E. J. Barbero, Int. J. Solids Struct. **31**, 2933 (1994).
[21] R. Luciano and E. J. Barbero, ASME J. Appl. Mech. **62**, 786 (1995).
[22] P. A. Fotiu and S. Nemat-Nasser, Int. J. Plast. **12**, 163 (1996).
[23] Gu Guo-Qing and R. Tao, Phys. Rev. B **37**, 8612 (1988).
[24] G. Q. Gu, J. Phys. D **26**, 1371 (1993).
[25] E. B. Wei, Y. M. Poon, F. G. Shin, and G. Q. Gu, Phys. Rev. B **74**, 014107 (2006).
[26] E. B. Wei, G. Q. Gu, and K. W. Yu, Phys. Rev. B **76**, 134206 (2007).
[27] T. Iwakuma and S. Nemat-Nasser, Comput. Struct. **16**, 13 (1983).
[28] Y. M. Strelniker and D. J. Bergman, Phys. Rev. B **50**, 14001 (1994).
[29] Z. Hashin and S. Shtrikman, Phys. Rev. **130**, 129 (1963).
[30] L. Rayleigh, Philos. Mag., Series 5, **34**, 481 (1892).
[31] D. R. McKenzie and R. C. McPhedran, Nature (London) **265**, 128 (1977).
[32] R. C. McPhedran and D. R. McKenzie, Proc. R. Soc. London, Ser. A **359**, 45 (1978).
[33] D. J. Bergman, Phys. Rev. B **14**, 1531 (1976).
[34] R. Courant, *Differential and Integral Calculus* (Interscience, New York, 1937).